September 1999 • NREL/SR-520-26882

Subcontractor Report

Thin-Film CIGS Photovoltaic Technology

Annual Technical Report, Phase I
16 April 1998 — 15 April 1999

A.E. Delahoy, D. Chorobski, F. Ziobro, and Z.J. Kiss
Energy Photovoltaics, Inc.
Lawrenceville, New Jersey

National Renewable Energy Laboratory

1617 Cole Boulevard
Golden, Colorado 80401-3393

NREL is a U.S. Department of Energy Laboratory
Operated by Midwest Research Institute • Battelle • Bechtel

Contract No. DE-AC36-98-GO10337

September 1999 • NREL/SR-520-26882

Thin-Film CIGS Photovoltaic Technology

Annual Technical Report, Phase I
16 April 1998 — 15 April 1999

A.E. Delahoy, D. Chorobski, F. Ziobro,
and Z.J. Kiss
Energy Photovoltaics, Inc.
Lawrenceville, New Jersey

NREL Technical Monitor: H.S. Ullal

Prepared under Subcontract No. ZAK-8-17619-21

National Renewable Energy Laboratory

1617 Cole Boulevard
Golden, Colorado 80401-3393

NREL is a U.S. Department of Energy Laboratory
Operated by Midwest Research Institute • Battelle • Bechtel

Contract No. DE-AC36-98-GO10337

NOTICE

Available to DOE and DOE contractors from:
Office of Scientific and Technical Information (OSTI)
P.O. Box 62
Oak Ridge, TN 37831
Prices available by calling 423-576-8401

Available to the public from:
National Technical Information Service (NTIS)
U.S. Department of Commerce
5285 Port Royal Road
Springfield, VA 22161
703-605-6000 or 800-553-6847
or
DOE Information Bridge
http://www.doe.gov/bridge/home.html


Printed on paper containing at least 50% wastepaper, including 20% postconsumer waste

Preface

Energy Photovoltaics, Inc. (EPV) has been engaged in the research and development of thin-film $CuInSe_2$ (CIS) and $Cu(In,Ga)Se_2$ (CIGS) PV manufacturing technology since 1991. During its previous 3-year research subcontract that ended in April 1998, EPV demonstrated a 9.7% CIGS minimodule and a 7.6%, 3100 cm^2, unencapsulated CIGS module that produced 24 watts [1]. EPV's approach to CIGS production may be characterized by the following descriptors: vacuum-based, glass substrate, novel source technology, high voltage cells, safety. These characteristics permit EPV to offer uniform, defect-free films; low substrate cost; reduced materials cost; reduced resistive losses; and production without major hazards. These features will translate to a reduced manufacturing cost.

EPV's manufacturing prowess may be gauged by examining its production of tandem junction, amorphous silicon PV modules. Under a multi-year, multi-megawatt contract with SMUD, these 40 watt modules are being delivered at a selling price of $\$2/W_p$ with no subsidies. The modules are listed by Underwriters Laboratories Inc. (UL). The current production level is 100 modules per day. Specialty, building-integrated PV modules (BIPV) have also been manufactured in a triple-laminate format and were installed as a replacement for spandrel glass on the south and east facades of the Conde Nast building at Four Times Square, NY [2].

The new subcontract is entitled "Thin-Film CIGS Photovoltaic Technology." The subcontract is part of the **NREL Thin-Film Partnership Program**, and EPV participates in the National CIS Team Meetings. The objective of this subcontract (ZAK-8-17619-21) is to demonstrate the control needed to reliably produce CIGS modules with powers in the 40 - 50 watt range for a substrate size of 4300 cm^2. In addition, the deposition processes need to be fast enough to be compatible with high throughput manufacturing. This document reports progress towards those goals during the first phase (April 16, 1998 - April 15, 1999) of this three-phase, cost-shared subcontract with NREL.

Acknowledgments

EPV wishes to acknowledge the diligent efforts and contributions of the EPV research, engineering, and support staff, including:

G. Butler, J. Camera, D. Chorobski, A. Delahoy (Principal Investigator), F. Faras, G. Jachura, Z. Kiss (Program Manager), R. Lyndall, B. Price, P. Ripish, A. Ruppert, F. Sheppard, H. Tedder, T. Varvar, F. Ziobro.

The following institutions are also acknowledged for their help and interest:

National Renewable Energy Laboratory	Brookhaven National Laboratory
Colorado State University	University of Illinois
Institute of Energy Conversion/Univ. of Delaware	Fraunhofer Institute

Summary

EPV, Inc.
Thin-Film CIGS Photovoltaic Technology
Subcontract no. ZAK-8-17619-21, Phase I

- EPV's new *FORNAX* process for CIGS formation shown to be capable of producing devices with high V_{oc} (>600 mV) and no dark aging effects. Parameters of the best device so far are V_{oc} 611 mV, J_{sc} 27.5 mA/cm^2, FF 74.5%, efficiency 12.5%.

- A 34 cm^2 16-cell minimodule was produced using *FORNAX* CIGS with V_{oc} 9.58 V, I_{sc} 52.0 mA, FF 69.8%, efficiency 10.2%.

- A new version of EPV's linear evaporation source was developed with improved rate and uniformity for Cu deposition over a width of 45 cm.

- Using the new linear source, the *FORNAX* process was implemented on 0.43 m^2 substrates in EPV's CIGS pilot line, with V_{oc} 537 mV and FF 70.3% being achieved on a device.

- The EPV Sub-Team of the National CIS R&D Team has produced Cd-free ZnO/CIGS devices on NREL CIGS using the *ROMEAO* process (reaction of metal and atomic oxygen) for ZnO deposition. After soaking, the best device exhibited a V_{oc} of 565 mV and an efficiency of 12.3%.

- Novel bias drive methods were devised for field soaking/anti-soaking experiments as a function of time and temperature. Scaling laws and an activation energy of 0.51 eV were found.

- Thermally stimulated capacitance reveals the existence of three distinct contributions to ZnO/CIGS device capacitance, two appearing to be gap state effects and one related to net doping concentration.

- The coating time of the sputtered pilot line ZnO:Al has been reduced by a factor of 3 while maintaining film quality. The deposition rate is 48 A s^{-1}.

- Plans are underway to increase the substrate size from 0.43 m^2 to 0.79 m^2.

Table of Contents

List of Figures

List of Tables

Introduction

Thin film photovoltaic modules based on $Cu(In,Ga)Se_2$ and related alloys have been shown to possess attributes that should enable them to compete effectively with modules based on crystalline silicon. And in due course, these attributes will allow realization of a lower $\$/W_p$ cost figure for CIGS relative to Xtl Si. These attributes are stability, reliability, high efficiency, and low materials cost. A part of the cost reduction and reliability of thin films results from monolithic integration, which avoids the handling and interconnection of a large number of fragile wafers.

On December 28, 1998, NREL achieved a new world record thin film solar cell efficiency following its sustained development of CIGS. The parameters of this cell are V_{oc} 678 mV, J_{sc} 35.1 mA cm^{-2}, FF 78.9%. However, no group in the US has fabricated a large module using the NREL 3-stage process because of the difficulties facing scale-up of this process.

To overcome these manufacturing barriers, Energy Photovoltaics, Inc. has developed vacuum equipment incorporating novel *linear evaporation sources* designed for uniform coating of large substrates. In addition, the equipment is capable of handling glass at the high temperatures necessary to produce the highest quality CIGS material *without glass warpage*. EPV's use of elemental selenium avoids the use of gaseous hydrogen selenide and provides for a *safe manufacturing environment*.

EPV's recent improvement of its Cu linear source has made it possible to implement its *FORNAX* CIGS process in its 0.43 m^2 pilot line. The versatility of this equipment is such that EPV can now in principle implement almost any vacuum-based CIGS process, including the NREL 3-stage process.

1.0 CIGS Formation by the *FORNAX* Process

EPV has employed three different CIGS absorber formation processes. These are reviewed in [3]. The first involved selenization of a sputtered, purely metallic precursor; the second, selenization of a Se-containing precursor prepared using separate evaporation and sputtering systems [4,5]; the third, termed the *FORNAX* process, is optimized for manufacturing and is carried out in a single machine. The *FORNAX* process appears to be a world-class process capable of producing CIGS cells with high V_{oc} (>600 mV) and a substantial lack of ageing or light-soaking effects [1,3].

The performance of cells produced in an R&D scale system by the new *FORNAX* process is shown in Table 1.1. This table compares the average and best device characteristics obtained with the *FORNAX* process to the average characteristics obtained with the well-optimized second process over an area of about 14 cm x 22 cm. An average V_{oc} of 569 mV was

obtained with the *FORNAX* process compared to 459 mV for the second process. The best *FORNAX* cell had a V_{oc} of 611 mV and FF of 74.5%, but a rather low current density of 27.5 mA/cm^2, despite the 2μm cell thickness. It is suspected that this material was too Cu poor. Nevertheless, because of the high cell voltages achieved, the *FORNAX* process appears to offer long term potential for exceptional cell efficiencies, and the higher band gap material is better suited to modules.

Table 1.1 Device characteristics obtained with CIGS from three different processes: EPV's 2nd and *FORNAX* processes, and NREL's 3-stage process.

CIGS process	Source of CIGS	Junction formation	V_{oc} (mV)	J_{sc} (mA/cm^2)	FF (%)	Effic. (%)
second	EPV (R&D)	CdS/ZnO (EPV)	459	37.0	69.1	11.7 <22>
FORNAX	EPV (R&D)	CdS/ZnO (EPV)	569	27.3	73.3	11.4 <24>
FORNAX	EPV (R&D)	CdS/ZnO (EPV)	611	27.5	74.5	12.5
FORNAX	EPV (pilot)	CdS/ZnO (EPV)	537	25.5	70.3	9.6
3-stage	NREL	CdS/ZnO (EPV)	628	35.9	74.1	16.7

FORNAX cells are also better behaved in terms of exhibiting no measurable degradation during storage (this has been checked up to 50 days) and only a small enhancement upon light soaking. Device 1761a6 was measured several times at 100 mW/cm^2 during a 3-hour light soak under short-circuit conditions. The sample was heat-sunk to an Al block with a silicone compound during the experiment. The fill factor increased initially with increasing light-exposure, and was then observed to decrease slightly for longer soaking times. It is possible that some slight heating of the sample occurred even though it was heat sunk. This is consistent with the slight drop in V_{oc} observed. The standard device characteristics as a function of light-exposure time are listed in Table 1.2 below.

Table 1.2 Light soaking of *FORNAX* device

soak time (s)	V_{oc} (V)	I_{sc} (mA)	FF (%)
3	0.600	5.86	71.7
5	0.598	5.92	72.9
41	0.596	5.80	72.9
174	0.594	5.70	73.1
477	0.592	5.83	73.3
1080	0.593	5.77	73.2
3483	0.589	5.85	72.6
10686	0.587	5.93	72.5

The I-V data were modeled and the series resistance and diode quality factor were extracted using the method of Sites and Mauk (*Solar Cells*, **27** (1989) 411-417). The series resistance was observed to drop from about 0.9 to 0.5 Ω-cm^2. A similar experiment performed on a device prepared from a selenized film (EPV's 2nd CIGS process) revealed a corresponding

drop in series resistance from 2.5 to 1.0 Ω-cm^2 [3]. Although both types of CIGS respond to light-soaking, the effect on device efficiency is stronger for the selenized CIGS film because the pre-light soak series resistance is large enough to significantly degrade the fill factor.

2.0 Mini-module Fabrication

A series of eight, 16-cell mini-modules was fabricated using *FORNAX* CIGS grown in an R&D scale system [3]. Cadmium sulfide was deposited by chemical bath deposition (CBD), and ZnO:Al by RF sputtering. Laser scribing was used for the Mo, while the 2nd and 3rd scribes were performed mechanically on a small x-y table. The I-V data for these mini-modules are shown in Table 2.1. An average V_{oc} of 607 mV per cell was obtained for one of the mini-modules. The difference in performance between the two runs is due to the different Ga/(In+Ga) ratio used in their preparation. The area lost at the interconnects is about 10%, so that the active area J_{sc} is about 27 mA/cm^2. The I-V curve of the best mini-module is shown below in Figure 2.1.

Table 2.1. Performance of unencapsulated mini-modules using *FORNAX* CIGS.

Module #	Area (cm^2)	V_{oc} (volts)	V_{oc}/cell (mV)	I_{sc} (mA)	J_{sc} (mA/cm^2)	FF (%)	P_{max} (mW)	Effic. (%)
1765a	38.0	8.77	548	56.7	23.9	65.9	325	8.63
1765b	36.4	8.97	561	53.5	23.5	67.0	312	8.84
1765c	34.8	8.52	532	53.2	24.5	63.8	284	8.31
1765d	36.0	8.91	557	52.1	23.2	66.3	302	8.56
1766a	34.0	9.58	599	52.0	24.5	69.8	332	10.24
1766b	29.7	8.46	604	51.3	24.1	67.9	291	9.89
1766c	33.6	9.48	593	50.4	24.0	68.3	308	9.71
1766d	33.6	9.71	607	50.6	24.1	69.2	322	10.1

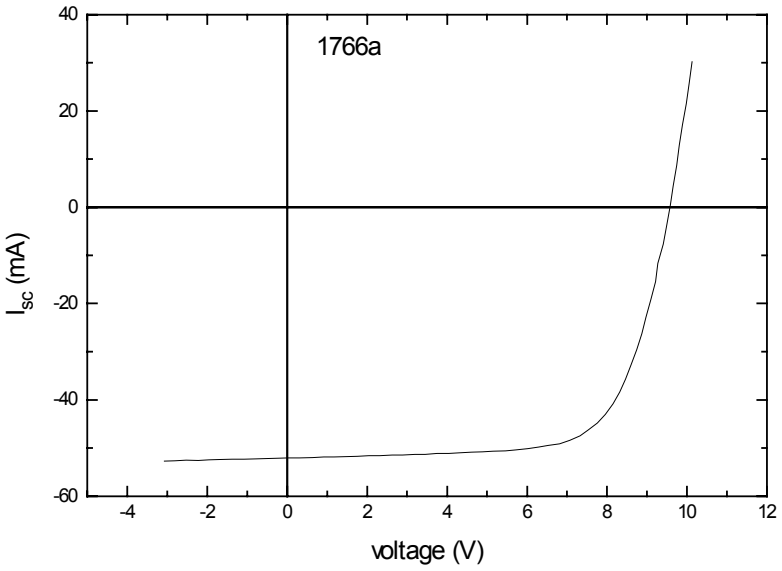

Figure 2.1 I-V curve of a 10.2% mini-module prepared using *FORNAX* CIGS

3.0 Pilot Line Implementation of the *FORNAX* Process

One of the principal objectives of this program is to successfully transfer an R&D scale, high efficiency CIGS process to manufacturing scale equipment in a manner that allows efficient production. The *FORNAX* process is not a selenization process, and requires co-deposition of Se with the other materials. The uniform supply of material in a hot, Se-containing atmosphere is non-trivial, and EPV has pioneered the use of linear evaporation sources to accomplish this [1, 3-6]. A major milestone is the demonstration of a well-controlled supply of Cu to the growing film by linear source evaporation.

Implementation of the *FORNAX* process on the pilot line has thus required development of a new version of linear source to allow better control of Cu deposition. Both rate and uniformity have been improved, and Figure 3.1 shows the thickness distribution achieved for a relatively thick deposition from the Cu linear source.

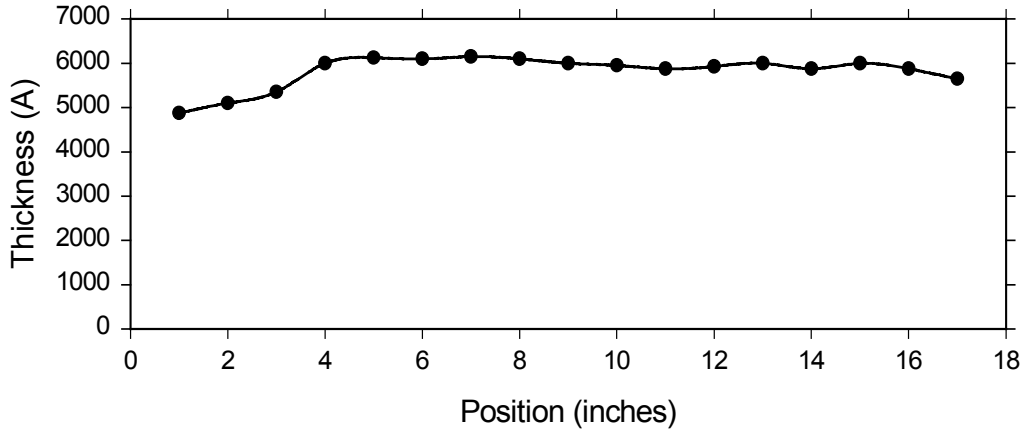

Figure 3.1 Film thickness distribution across the narrow dimension of a 0.43 m^2 glass substrate (perpendicular to the direction of substrate travel) after Cu deposition from a linear source; T_{source} 1580 °C, time 20 min.

EPV is also capable of forming compound materials in the pilot line system by using multiple linear sources. Figure 3.2 shows, for example, the thickness distribution of a film of $(In,Ga)_xSe_y$ prepared using multiple sources.

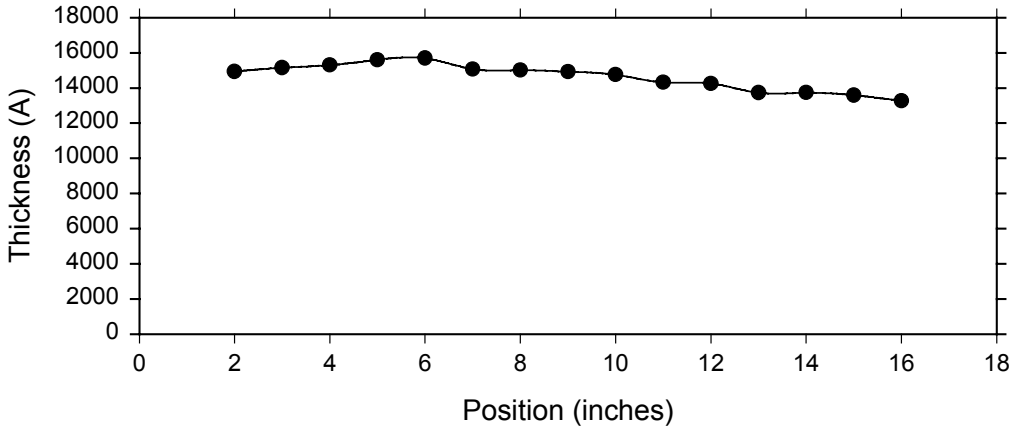

Figure 3.2 Thickness distribution for $(In,Ga)_xSe_y$ formed by linear source evaporation (time 5 min).

The dependence of thickness on measured source temperature is shown in Figure 3.3 for both the high temperature Cu source and for two different versions of a lower temperature source, in this case for evaporation of a III-V compound. Here, a time averaged deposition rate across the full plate as high as 50 A/s is demonstrated, with the instantaneous deposition rate in the region of deposition being an order of magnitude higher. The dashed curve is scaled from $P/\sqrt{T_s}$, where P is the vapor pressure of Cu at temperature T_s (°K); this quantity is proportional to evaporation rate (v.p. data from Maissel and Glang).

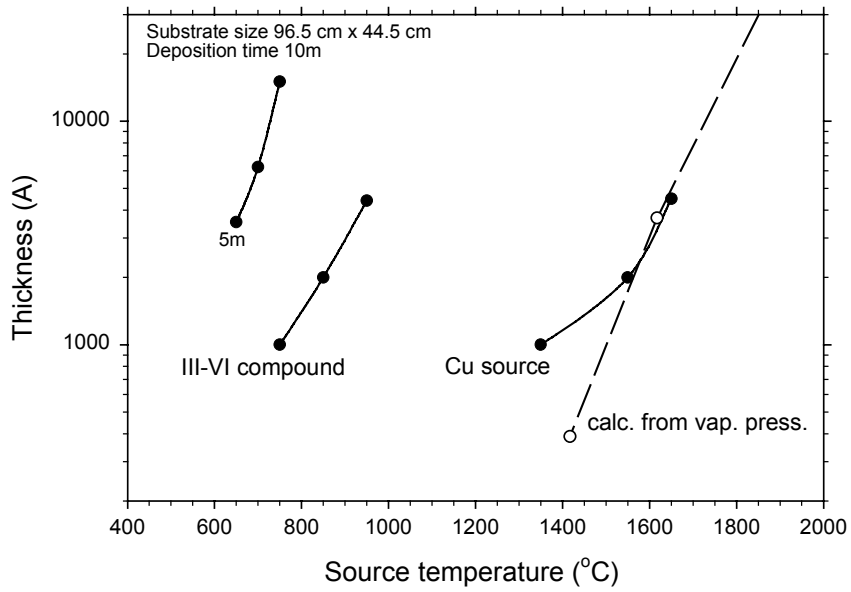

Figure 3.3 Thickness versus source temperature for Cu and typical III-VI sources

Devices produced on CIGS material grown in the pilot line by the *FORNAX* process on 0.43 m^2 (96.5 x 44.5 cm^2) soda lime glass substrates using linear source evaporation have exhibited good voltages and fill factors. The I-V parameters for such a device are shown in the 4th entry in Table 1.1 above. The open-circuit voltage was 537 mV and FF 70.3%. Better control of the Cu/(In+Ga) ratio, Ga profile, and Na incorporation in the pilot line CIGS should enable higher current densities to be obtained.

4.0 Cd-free Junction Formation

While junction formation is routinely accomplished via chemical bath deposition of CdS, during Phase I of this subcontract EPV initiated a new program to explore direct deposition of ZnO on small samples of CIGS using a novel growth technique for the ZnO, viz. the reaction of fluxes of Zn and atomic oxygen [7]. This method of deposition is termed the *ROMEAO* technique (Reaction of Metal and Atomic Oxygen).

This new program was announced at the National CIS R&D Team Meeting (Denver, Sept. 1998) and the collaboration of NREL was invited. EPV had developed the reactive ZnO under a DOE SBIR award. Some of the goals of this program are: 1) to eliminate Cd, and develop a dry junction formation process, 2) to develop a CIGS/reactive ZnO/sputtered ZnO process for short term manufacturing purposes, and 3) to further understand junction formation and metastable effects in direct junction devices.
The underlying mechanisms have yet to be elucidated.

Using CIGS provided by Miguel Contreras, NREL, direct junctions were formed by the simultaneous supply of fluxes of Zn and atomic oxygen (AO). The AO source consisted of a quartz tube fitted with external electrodes into which O_2 was introduced and excited by RF, the discharge products exiting through a small hole. [7]. The CIGS was generally used without any cleaning, and the substrate temperature was about 145-150 °C. The resulting cells exhibit a variety of light soaking effects, the most noticeable being an increase in V_{oc}. An increase in fill factor is also usually observed. The changes are rapid at first, but can continue at a reduced rate for long times. The effects relax in the dark. It was found that the improvement can also be induced by forward voltage bias, regardless of whether light is present.

Examples of the I-V curves obtained before and after soaking are shown in Figure 4.1 below for cells C1067-60 and C1080-73b. Initial V_{oc}'s can range from 100 mV to 400 mV+. It is very encouraging that a V_{oc} of 565 mV has been observed (see Figure 4.1, C1080-73b). This cell exhibited an efficiency of 12.3% after soaking.

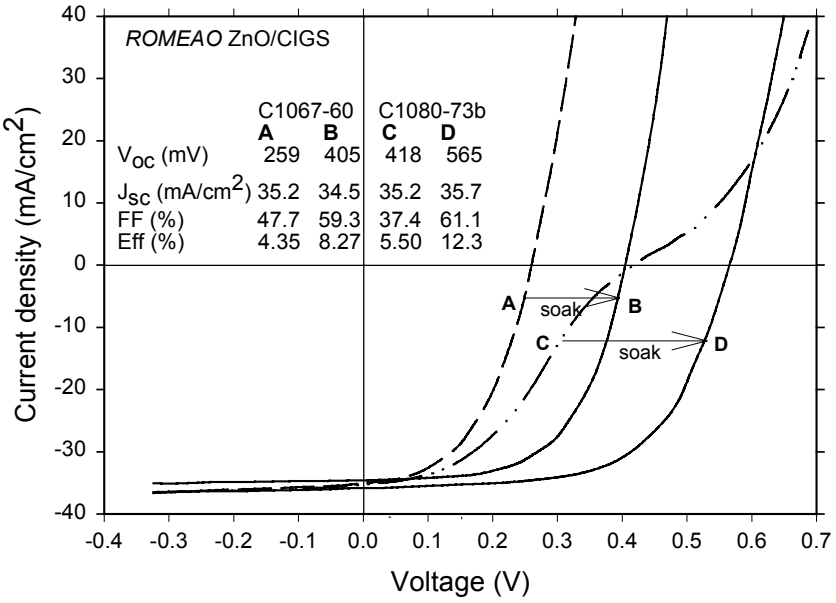

Figure 4.1 I-V curves before and after soaking for two Cd-free, ZnO/CIGS devices (ZnO prepared by the *ROMEAO* process).

To a first approximation, there is usually no observable change in J_{sc} upon soaking. In some cases however, after anti-soaking by application of reverse bias, the I-V curve is so degraded that the full photocurrent is collected only for reverse voltages less than some negative value. In such cases J_{sc} is reduced. In other cells, anti-soaking appears to almost eliminate the junction barrier or band bending, so that the devices barely rectify.

A plot of V_{oc} versus illumination time at three different temperatures is shown in Figure 4.2. The irradiance was 100 mW/cm^2. It is found that the V_{oc} versus log(t) curves can be described by a stretched exponential. For example, the room temperature data of Figure 4.2 is fairly well described by the equation

$$V_{oc}(t) = 255 + 240\{1-\exp(-t/800)^{0.5}\} \text{ mV}$$

Whether this has physical significance is not clear. For example, is the $t^{0.5}$ component (suggesting diffusion) an accident? It does appear, however, that the underlying mechanism possesses a wide range of time constants. The V_{oc} vs. log(t) curves also scale with t.exp(-E/kT) as a parameter, with E = 0.51 eV. Again, whether E can be interpreted as a trap depth (either for electronic energy states, or grain boundary diffusion) is not clear.

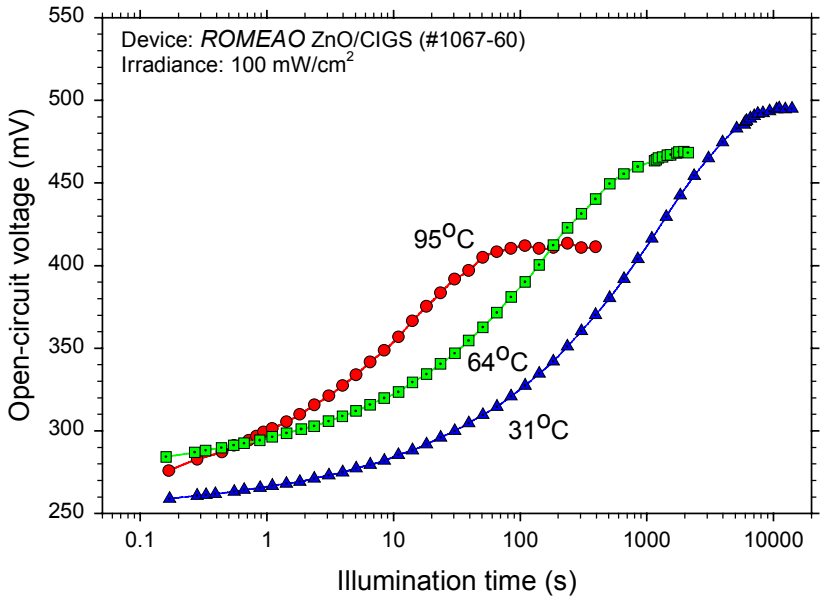

Figure 4.2 V_{oc} versus log time for a *ROMEAO* ZnO/CIGS device at three temperatures, showing earlier achievement of saturation at elevated temperatures.

The elevated V_{oc} can be returned to its initial value by application of zero bias. By application of reverse bias, the V_{oc} can be driven below its dark rest value. Although, in general, the value of V_{oc} is not sufficient to fully characterize the state of the device (since the state depends on the detailed history of the bias condition), it appears that the device can be brought to a well-defined state by waiting until t = infinity at a fixed bias.

With these notions in mind, we established the following "**drive and interrogate**" procedure. Steady state is attained through prolonged soaking at a first voltage bias, and then the device is driven by switching to a second voltage at t = 0, with the condition of the device being interrogated by brief (low light) measurement of V_{oc} at various times for t > 0. Two data sets spanning the temperature range 31 - 125 °C were acquired, and are shown in Figure 4.3. In one set, the 1st and 2nd bias conditions are -0.4V and a positive bias (device V_{oc} improved by soaking), and in the other set a positive bias and -0.4V (device V_{oc} decreased by anti-soaking). The device was interrogated by briefly opening reed relay contacts to remove the bias condition and open circuit the device. The irradiance was 12 mW/cm^2 and the data was acquired by computer at logarithmically increasing times, in some cases with manual override at long times to verify that a steady state condition had truly been achieved. These dramatic data show that V_{oc} can be driven up or down by bias condition, and that the effect is greatly accelerated at elevated temperatures.

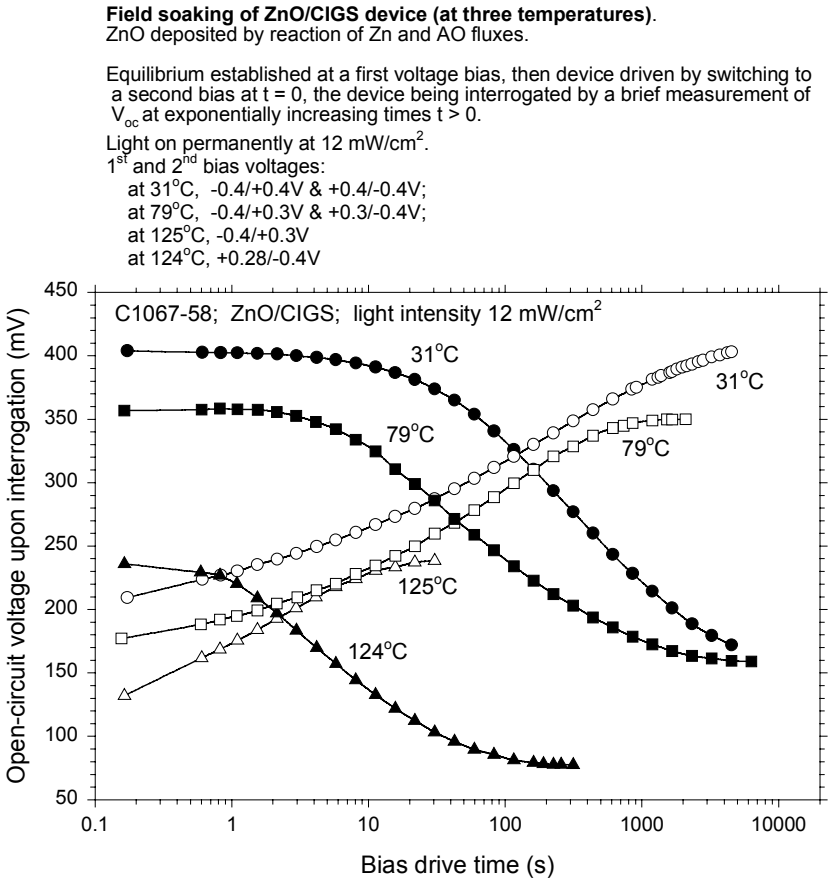

Figure 4.3 Field soaking of ROMEAO ZnO/CIGS device between two steady states defined by different applied voltage biases

While most devices require about 10,000 seconds to reach steady state at room temperature, it has now been confirmed that some reach a steady state faster. This is illustrated in Figure 4.4, which shows a field soak experiment conducted at 0.6V bias (forward direction) with V_{oc} sampled periodically by opening relay contacts to remove the bias. Steady state is achieved in about 200 s.

At the time of writing the bias effect appears reversible, although experiments have not yet been conducted to demonstrate (or otherwise disprove) exact reversibility. This is an important point, since while we started by assuming that the effects are due to the changing of deep state occupancy in the space charge region by Fermi level shift, it has been suggested that Cu electromigration may play a role. It is our opinion that electromigration is unlikely to exhibit perfect reversibility such as would be expected from purely electronic effects.

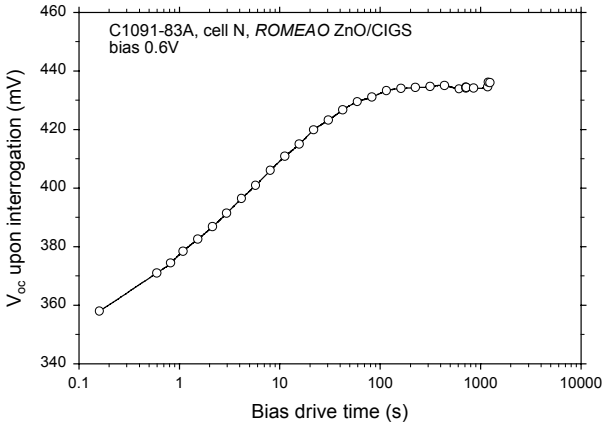

Figure 4.4 Field soaking of a "fast" device

Through partial soaking/anti-soaking/soaking sequences it is possible to obtain $V_{oc}(t)$ curves that intersect, thereby demonstrating that the state of the sample cannot in general be specified by a single parameter such as V_{oc}.

Some remarkable re-scaling features are present in the behavior of most devices. Figure 4.5 shows field soaking data as obtained by the "drive and interrogate" procedure applied to different pairs of initial and final steady states. Curve A shows V_{oc} upon interrogation while driving at +0.2V bias almost to saturation from the 0V rested condition. Next, from this steady state, +0.4V was applied (curveB). Curve C is the V_{oc} data obtained by driving back to +0.2V, and shows the asymptotic approach to the same steady state V_{oc} exhibited by curve A. After allowing the sample to relax at 0V, curve D was obtained by driving at 0.4V. It was discovered that curve A and curve D represent the same behavior in time and differ only in vertical scaling. Thus if the V_{oc} data of curve A, $V_A(t)$, is scaled to expand its range by a factor k, the resulting data $V_S(t)$ is found to almost exactly reproduce curve D data by appropriate choice of k:

$$V_S(t) = k[V_A(t) - V_A(0)] + V_A(0) = V_D(t) \quad !!$$

$V_S(t)$ is plotted in Figure 4.5 using open squares, and is seen to overlay $V_D(t)$. Thus field soaking at a higher voltage does not accelerate the progress to steady state. Furthermore, re-scaling of curve B can *also* generate the same curve:

$$V_{S'}(t) = k'[V_B(t) - V_B(0)] + V_A(0) = V_D(t)$$

This curve is plotted using triangles, and also overlays V_D. In other words, the evolution in time between two steady states does not depend on the initial and final bias conditions.

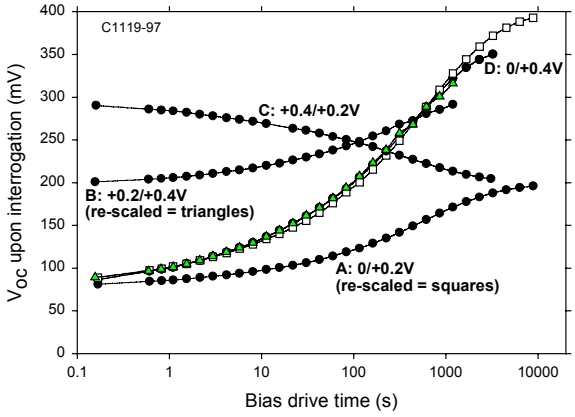

Figure 4.5 Field soaking experiments and re-scaling of V_{oc}

A dramatic demonstration that the V_{oc} of a sample in a non-steady state does not uniquely specify that state is afforded by the following experiment. First, the sample was field-soaked from its 0V steady state at 0.2V bias to steady state, thereby achieving a $V_{oc}(0.2V)$ upon interrogation. Next, the sample was allowed to relax at 0V. Then the sample was field-soaked at 0.65V until its V_{oc} upon interrogation reached $V_{oc}(0.2V)$. At this point, call it t = 0, the applied bias was switched to 0.2 V, and $V_{oc}(t)$ was measured for t > 0. Note that at t = 0 the sample is biased at 0.2V and exhibits $V_{oc}(0.2V)$. Should the sample continue to exhibit this V_{oc} without change, as it did after reaching steady state in the first step? The data is shown in Fig. 4.6. The V_{oc} initially fell rapidly, and then climbed slowly. This difference in behaviour in time from a starting $V_{oc}(0.2V)$ under identical conditions (applied bias 0.2V) clearly demonstrates that the initial states were in fact different.

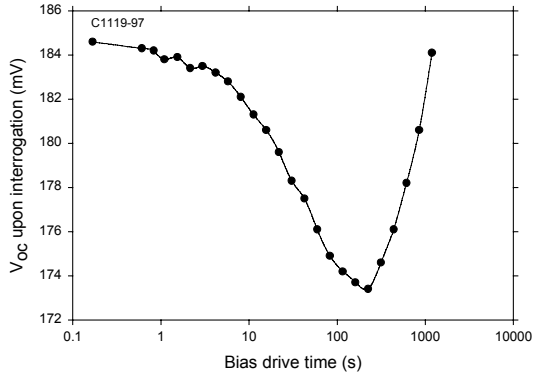

Figure 4.6 Field soaking after change of bias condition at t = 0 in a non-steady state. (experiment sequence: drive from the 0V steady state at 0.65V until V_{oc} equals that produced by driving at 0.2V to steady state ($V_{oc}(0.2V)$); at this point (t = 0) switch applied bias to 0.2V and interrogate V_{oc} for t > 0)

Figure 4.7 shows the data of Fig. 4.6 re-plotted, together with part of the data (for the same sample) from Fig. 4.5 for the field soak at 0.2V starting from the 0V relaxed state. The data of Fig. 4.6 has been shifted in time before plotting to reveal that its long time tail is in fact identical to the approach to steady state for the 0V/+0.2V field soak. Is this a coincidence? No. The interpretation is that once the short time scale changes induced by the 0.65V soak are erased by waiting for times longer than the time during which the 0.65V was applied, the sample has memory only of the long time scale features of the 0V relaxed state, and therefore must evolve in time identically in its progression to steady state at 0.2V applied.

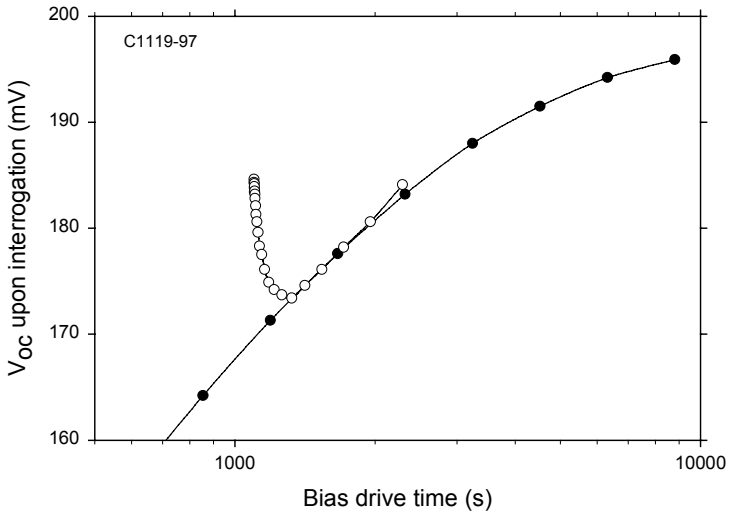

Figure 4.7 Coincidence of long time tails for two 0.2V field soaks; closed circles: 0/0.2V soak data from Fig. 4.5; open: data of Fig. 4.6 replotted after time translation.

Finally, although almost all samples fabricated by depositing *ROMEAO* ZnO onto CIGS exhibit light and field soaking effects, at least one sample has been found that is relatively stable. Thus Figure 4.8 shows field soak data for sample C1103-88 driven at 0.65V applied bias with V_{oc} interrogated up to 1200 s. No definite change is observed within the resolution of the experiment. This experiment was repeated a month later with a similar result. The reason for this sample's stability is not known, and the stability has not yet been duplicated in any other sample.

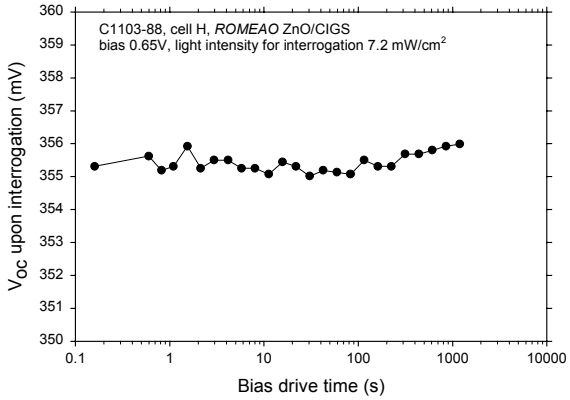

Figure 4.8 Existence proof for a *ROMEAO* ZnO/CIGS device that does not soak

We have started to examine the changes induced in these devices by light soaking and field soaking using capacitance measurements performed at 100kHz. Figure 4.9 shows the dependence of capacitance upon applied bias plotted in the usual manner of $1/C^2$ *vs*. V for a CdS-containing device in the configuration *ROMEAO* ZnO/CdS/CIGS. At room temperature there are contributions to the capacitance from gap states; this effect is minimized by performing the measurements at liquid nitrogen temperatures to freeze out the contribution of deep states. The plot is also changed by light soaking the device at 70°C, cooling with the light on, and then turning the light off to perform the C *vs.* V measurement. In this case the slope of the plot $d(1/C^2)/dV$, which is proportional to the inverse of the net doping density, is reduced, implying a higher space charge density. The equation for the net doping density is

$$N_A - N_D = -(2/q\varepsilon)\,[d(1/(C/A)^2)/dV]^{-1}$$

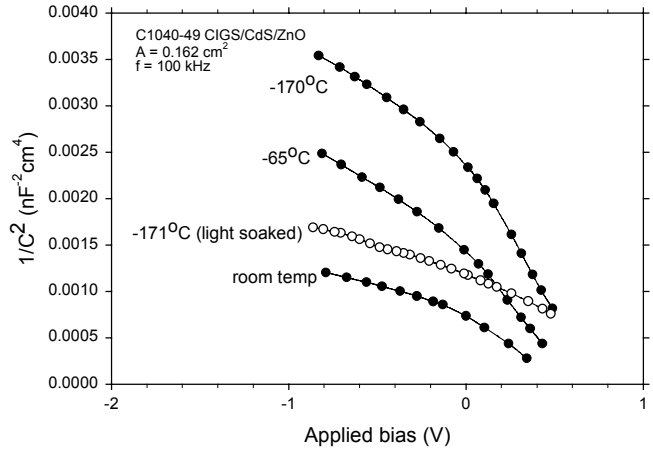

Figure 4.9 Capacitance ($1/C^2$) versus voltage plot for a ZnO/CdS/CIGS device

The behavior of a CdS-free device is similar, and is shown in Figure 4.10. The magnitude of the net doping density is, however, smaller, being 2.5 x 10^{15} cm^{-3} in the dark and 5 x 10^{15} in the light, compared to the more favorable 1.5 x 10^{16} in the light for the CdS-containing device.

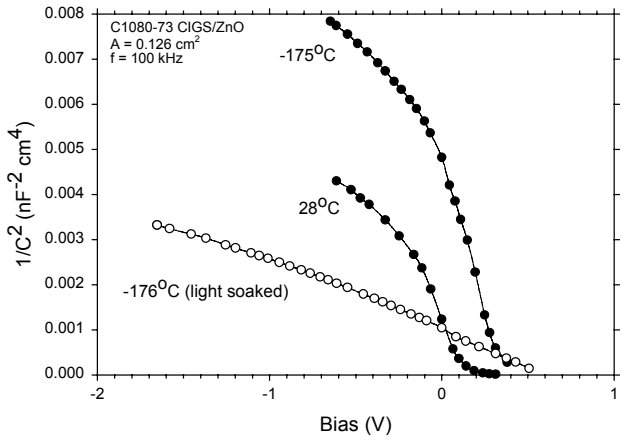

Figure 4.10 Capacitance ($1/C^2$) versus voltage plot for a ZnO/CIGS device

Transient capacitance measurements were also performed in the usual manner to detect majority carrier traps [8]. In this experiment the CdS-free device was biased at -0.7V and allowed to reach steady state, corresponding to emptying of the traps. The bias was then reduced to zero for 10 seconds to allow traps to fill with majority carriers (holes). Then the bias was returned to -0.7V and the capacitance was recorded versus time. Figure 4.11 shows the transient capacitance $\Delta C(t) = C(t) - C(\infty)$.

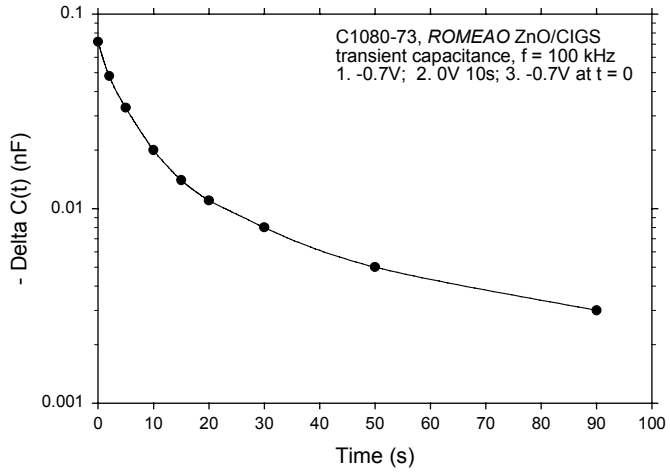

Figure 4.11 Transient capacitance (-ΔC) *vs.* time

Note that ΔC is negative, signifying a widening of the space charge region i.e. addition of positive charge to counteract the negative space charge of acceptors. The addition of positive charge implies hole trapping. The emission of trapped holes would normally be described by $dp_t/dt = -e_p p_t$ where e_p is the emission rate. The non-exponential decay evident from Figure 4.11 suggests a distribution of hole trap levels.

Thermally stimulated capacitance (TSCAP) measurements were also performed. In the baseline scan (closed circles in Figure 4.12) a reverse bias of -0.5V was applied to empty any traps and the device was cooled. Upon warming, the C(T) curve exhibited in the figure was obtained. The step in capacitance around -100°C (superimposed on the gradual upwards slope) implies E_F must cross a defect state. A forward bias of 0.3V was then used to inject both electrons and holes during the next cooling cycle. Upon warming (again under a reverse bias of -0.5V), the C(T) curve plotted with open circles in Figure 4.12 was obtained.

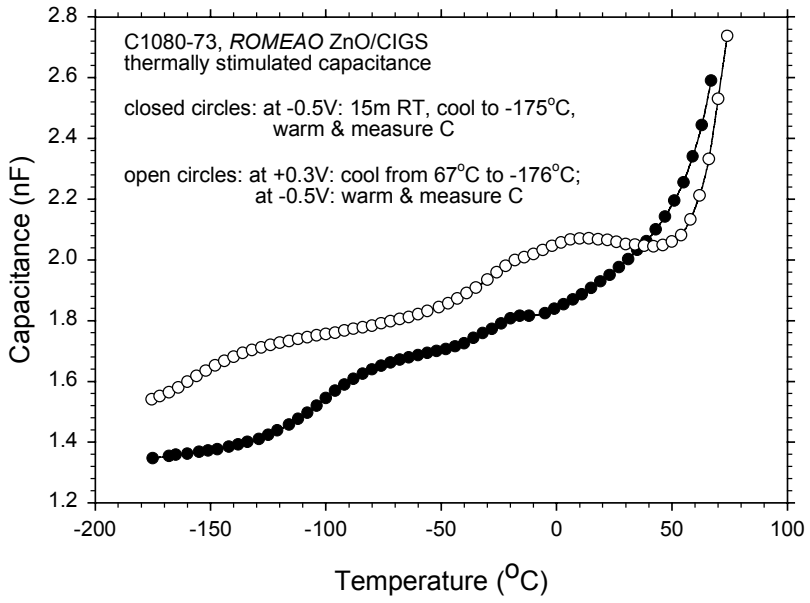

Figure 4.12 Thermally stimulated capacitance

Two new features appear in this curve, including a decline in capacitance in the range 10-40°C. This could signify electron emission from traps, or more generally, an anti-soaking effect that erases the +0.3V field soak with a corresponding widening of the space charge region. The anti-soaking effect, as alluded to earlier, could involve electromigration. Possible species are Cu^+, O^-, Zn or Na. Forward bias may also promote diffusion and clustering of point defects to yield neutral and inactive $[V_{Cu}\ In_{Cu}\ V_{Cu}]^0$ with cluster breakup occurring otherwise [9].

The above results will be presented at the European MRS Spring Meeting in Strasbourg [10].

5.0 Molybdenum and Zinc Oxide Process Development

Most of EPV's CIGS modules have been prepared using its standard recipe for the Mo back contact layer as summarized in Table 5.1. In this bi-layer recipe, the first layer exhibits good adhesion, but poor electrical conductivity, while the second layer exhibits improved conductivity, but increased internal stress. Other factors of importance are the quality of the glass washing, and whether the tin side or the fire side of the glass is used. This particular recipe utilizes the fire side. The resulting sheet resistance is about 1.3 Ω/square. The instantaneous deposition rate (averaged over the target width) is calculated from the equation:

deposition rate = (thickness/scan) / (time under target/scan)

where time under target per scan is the time taken by an element of the substrate to pass under the target. Other quantities of interest are the dynamic deposition rate (DDR), defined as the thickness (in A) x scan speed (cm/s), and the specific deposition rate (r_{sp}) defined as the volume of material (in $A.cm^2$) per joule supplied. The relationship between these quantities is r_{sp} = DDR x L_r/P, where L_r is the length of the racetrack (in cm) and P is the sputtering power (W). The DDR and r_{sp} are also shown in Table 5.1.

Table 5.1 Sputtering parameters for Mo back contact layer

	Power W	Press mTorr	Volts V	Amps A	Scan time min	Power density W/cm^2	Thickness µm	Dep. rate A/s	DDR Acm/s	r_{sp} Acm^2 /J
layer 1	2100	20	281	7.5	6	3.7				
layer 2	2100	14	296	7.1	6	3.7				
overall							0.43	57	576	15.3

Experience has shown that while the Mo layer may initially appear to be adherent, problems can occur at a later stage of processing, e.g. after laser scribing, CIGS deposition, CBD CdS, or ZnO deposition. The recipe shown above is currently being upgraded to provide enhanced adhesion, lower sheet resistance, and appropriate Na transmission.

Assuming Al-doped ZnO is used as the transparent conductor in CIGS modules, then our earlier analyses indicated that reactive sputtering of a metallic target offered promise for meeting the high deposition rates required for high volume manufacturing. However, since sputtering from a ceramic target may offer greater process simplicity and reproducibility, we have decided to explore the upper limits of deposition rate for such ceramic targets. During the last subcontract a sputtering power of 1150 watts was used for deposition from the ceramic target. This has been increased to 3880 watts during Phase I of this subcontract, thereby allowing the number of passes of the module past the target to be reduced from 6 to 2. The sputtering parameters of the new process are summarized in Table 5.2. The increase in sputtering power resulted in an increase of deposition rate from 13 A/s to 48 A/s, as

averaged over the width of the target. No target problems have been encountered so far at the increased power density.

Table 5.2 Higher rate sputtering parameters for $ZnO:Al_2O_3$

	Old process	New process
Sputter gas	Ar/O_2	Ar/O_2
Voltage	525 V	560 V
Current	2.19 A	6.93 A
Power	1150 W	3880 W
Power density	2.0 W/cm^2	6.8 W/cm^2 (averaged over target area)
Pressure	2 mTorr	3 mTorr
Scan time	20 minutes	20 minutes
Number of scans	6	2
Film thickness	1.0 μm	1.2 μm
Deposition rate	13 A/s	48 A/s (averaged over target width)

The increased deposition rate necessitated a re-optimization of the fraction of oxygen added to the argon sputtering gas. Figure 5.1 shows the combinations of sheet resistance and white light transmission that were obtained as the oxygen concentration was varied. The best combination of properties is similar to that obtained by the old process.

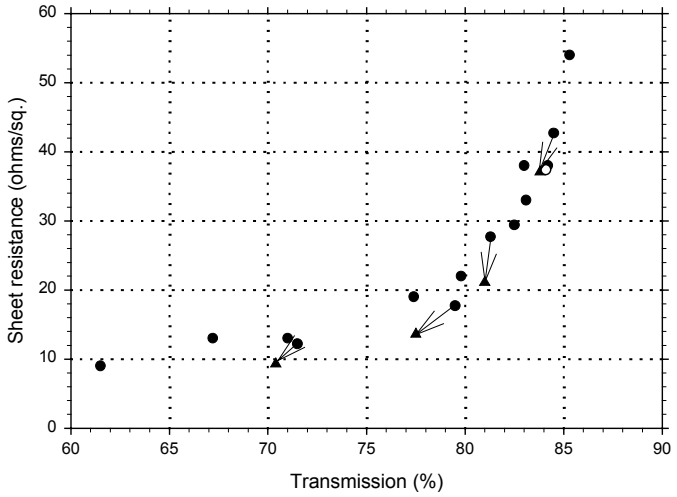

Figure 5.1 Zinc oxide film parameters for various oxygen concentrations, and after annealing

By annealing the films in air at 150°C useful increase in conductivity could be obtained, albeit with a slight decrease in transmission. These changes are indicated by arrows in Figure 5.1, and represent annealing times of 64 - 231 hours.

The dependence of film conductivity and white light transmission on oxygen flow is shown in Figure 5.2. As the oxygen flow is increased, the conductivity falls while the transmission increases. The relationship is not unique, since the state of the target depends on its prior history of oxygen exposure. From prior modeling experience, a ZnO:Al film conductivity of about 375 S/cm is set as the target value for the new ZnO process for yielding the highest module efficiency.

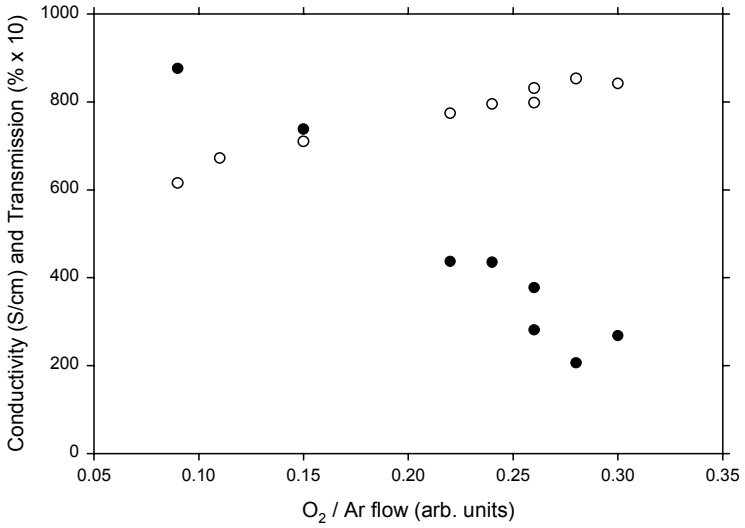

Figure 5.2 ZnO film conductivity and transmission as a function of oxygen flow

Future Plans

Our most important goals for Phase II include:

a) the improvement of CIGS compositional uniformity across the width of the plate,
b) the improvement of flux monitoring accuracy,
c) optimization of Mo and Na content,
d) a renewed focus on junction formation, including parallel work on streamlining the CBD CdS, on vacuum deposited buffer layers, and on in-situ junction formation,
e) clear demonstration of reproducibility for cell and module efficiencies

Conclusions

Using a new CIGS formation process, termed the *FORNAX* process, 16-cell minimodules were prepared with efficiencies up to 10.2% and cell voltages averaging 607 mV. The successful operation of an improved type of linear source for Cu delivery has allowed implementation of the *FORNAX* process in the pilot line on 96.5 cm x 44.5 cm glass substrates. The significance of this accomplishment is that a pilot scale CIGS formation machine of extreme versatility has been constructed, one that is capable of emulating all known vacuum CIGS processes. We look forward to trials and engineering development of this new source, and renewed efforts on the module front using this machine.

Several interesting results have been obtained in preparing CdS-free, ZnO/CIGS junctions by a new method utilizing Zn and atomic oxygen fluxes. A cell efficiency of 12.3% was achieved, and remarkably strong light and field soaking effects were observed.

References

1. "CIS Photovoltaic Technology", A.E. Delahoy, J.S. Britt, and Z.J. Kiss *Final Technical Report, NREL/SR-520-25713. 29pp. Available NTIS, Springfield, VA* (1998).
2. "Building-Integrated Amorphous Silicon at Four Times Square," G.J. Kiss, A.E. Delahoy, Z.J. Kiss, A. Varvar, F. Ziobro, *Proceedings of the 2nd World Conference and Exhibition on Photovoltaic Solar Energy Conversion*, Vienna, Austria, 6-10 July 1998 (European Commission, Ispra, 1998) pp. 2452-2456.
3. "Baseline Process Development for Pilot Line Production of CIGS Modules," A.E. Delahoy, D. Chorobski, F. Ziobro, Z.J. Kiss, *NCPV Photovoltaics Program Review; Proceedings of the 15th Conference, Denver, CO, 1998*; *AIP Conf. Proc. Vol. 462* (AIP, NY, 1999) pp. 144-151.
4. "Large-Area Coating of CIGS and ZnO for Photovoltaics", J.S. Britt, A.E. Delahoy, and Z.J. Kiss, *Conference Record of the 14th European Photovoltaic Solar Energy Conference,* Barcelona, Spain, (H.S. Stephens, 1997), pp. 1287-1290.
5. "Pilot Production of CIGS Photovoltaic Modules", J.S. Britt, A.E. Delahoy, and Z.J. Kiss, *Proceedings of the 26th IEEE Photovoltaic Specialists Conference* (IEEE, 1997) pp.335-338.
6. "Thin-Film PV Modules: Manufacturing Technology and Issues". A.E. Delahoy and P.V. Meyers. *Tutorial III, September 29, 1997; 26th IEEE Photovoltaic Specialists Conference; Anaheim, CA.* (1997).
7. "Zinc Oxide Film Formation using Atomic Oxygen and Metal Flux Sources," A.E. Delahoy, and A.F. Ruppert, *Proceedings of the 2nd World Conference and Exhibition on Photovoltaic Solar Energy Conversion*, Vienna, Austria, 6-10 July 1998 (European Commission, Ispra, 1998) pp. 668-671.
8. "Capacitance Transient Spectroscopy," G.L. Miller, D.V. Lang, and L.C. Kimerling in *Ann. Rev Mater. Sci. 1977, 377-448* (Annual Reviews Inc., Palo Alto, CA).
9. "The Electronic Effects of Point Defects in $Cu(In_xGa_{1-x})Se_2$ Devices," A. Rockett *NCPV Photovoltaics Program Review; Proceedings of the 15th Conference, Denver, CO, 1998*; *AIP Conf. Proc. Vol. 462* (AIP, NY, 1999) pp. 132-137.
10. "Charging and Discharging of Defect States in CIGS/ZnO Junctions," A.E. Delahoy and A.F. Ruppert, E-MRS, Strasbourg, France, June 1-4 , 1999.

REPORT DOCUMENTATION PAGE

Form Approved
OMB NO. 0704-0188

1. AGENCY USE ONLY (Leave blank)	2. REPORT DATE	3. REPORT TYPE AND DATES COVERED
	September 1999	Annual Technical Report, Phase I; 16 April 1998 – 15 April 1999

4. TITLE AND SUBTITLE
Thin-Film CIGS Photovoltaic Technology; Annual Technical Report, Phase I; 16 April 1998 – 15 April 1999

5. FUNDING NUMBERS
C: ZAK-8-17619-21
TA: PV905001

6. AUTHOR(S)
A.E. Delahoy, D. Chorobski, F. Ziobro, and Z.J. Kiss

7. PERFORMING ORGANIZATION NAME(S) AND ADDRESS(ES)
Energy Photovoltaics, Inc.
276 Bakers Basin Road
Lawrenceville, NJ 08648

8. PERFORMING ORGANIZATION REPORT NUMBER

9. SPONSORING/MONITORING AGENCY NAME(S) AND ADDRESS(ES)
National Renewable Energy Laboratory
1617 Cole Blvd.
Golden, CO 80401-3393

10. SPONSORING/MONITORING AGENCY REPORT NUMBER
SR-520-26882

11. SUPPLEMENTARY NOTES
NREL Technical Monitor: H.S. Ullal

12a. DISTRIBUTION/AVAILABILITY STATEMENT
National Technical Information Service
U.S. Department of Commerce
5285 Port Royal Road
Springfield, VA 22161

12b. DISTRIBUTION CODE

13. ABSTRACT *(Maximum 200 words)*

This report describes work performed by Energy Photovoltaics, Inc. (EPV) under Phase I of this subcontract. EPV's new *FORNAX* process for CIGS formation is capable of producing devices with high V_{oc} (>600 mV) and no dark aging effects. Parameters of the best device so far are V_{oc} = 611 mV, J_{sc} = 27.5 mA/cm^2, FF = 74.5%, and efficiency = 12.5%. A 34-cm^2 16-cell minimodule was produced using *FORNAX* CIGS with V_{oc} = 9.58 V, I_{sc} = 52.0 mA, FF = 69.8%, and efficiency = 10.2%. A new version of EPV's linear evaporation source was developed with improved rate and uniformity for Cu deposition over a width of 45 cm. Using the new linear source, the *FORNAX* process was implemented on 0.43-m^2 substrates in EPV's CIGS pilot line, with V_{oc} = 537 mV and FF = 70.3% being achieved on a device. The EPV Subteam of the National CIS R&D Team has produced Cd-free ZnO/CIGS devices on NREL CIGS using the *ROMEAO* process (reaction of metal and atomic oxygen) for ZnO deposition. After soaking, the best device exhibited a V_{oc} of 565 mV and an efficiency of 12.3%. Novel bias drive methods were devised for field soaking/anti-soaking experiments as a function of time and temperature. Scaling laws and an activation energy of 0.51 eV were found. Thermally stimulated capacitance reveals the existence of three distinct contributions to ZnO/CIGS device capacitance, two appearing to be gap-state effects and one related to net doping concentration. The coating time of the sputtered pilot-line ZnO:Al has been reduced by a factor of 3 while maintaining film quality. The deposition rate is 48 A s^{-1}. Plans are under way to increase the substrate size from 0.43 m^2 to 0.79 m^2.

14. SUBJECT TERMS
photovoltaics ; thin films ; Thin-Film PV Partnership Program ; CIGS modules ; FORNAX process ; minimodule fabrication ; ROMEAO process

15. NUMBER OF PAGES
30

16. PRICE CODE

17. SECURITY CLASSIFICATION OF REPORT	18. SECURITY CLASSIFICATION OF THIS PAGE	19. SECURITY CLASSIFICATION OF ABSTRACT	20. LIMITATION OF ABSTRACT
Unclassified	Unclassified	Unclassified	UL